LANGMUIR

pubs.acs.org/Langmuir Article

A Wide-Spectrum Oil/Water Separation Scenario Enhanced by a Chitosan-Based Superwetting Membrane with a Tunable Microstructure and Powerful Photocatalytic Self-Cleaning Capability

Hanbing Zhu, Yi Song, Haowen Qing, Mengying Liu, Yanning Zhao, Mingbo Wu, and Zhaoxuan Feng*

Cite This: *Langmuir* 2025, 41, 633−645 Read Online

ACCESS | Metrics & More | Article Recommendations | Supporting Information

ABSTRACT: Oil spills and industrial oily wastewater pose serious threats to the environment. A series of modified membranes with special wettability have been widely used for separating oil/water mixtures and emulsions. However, these membranes still face challenges such as the detachment of the modified coatings and membrane fouling. Here, a freestanding biobased superwetting nanofibrous membrane for oil/water mixture separation was electrospun with chitosan (CS) and poly(vinyl alcohol) (PVA) as precursors, followed by chemical cross-linking and in situ growth of β-FeOOH nanoparticles on the surface. Moreover, by precisely controlling both the cross-linking time between CS and PVA and the growth time of β-FeOOH nanoparticles, the nanosize apertures and rough structures on the membrane surface can be regulated toward a wide range of oil/water separation scenarios. As a result, FeOOH@CS/PVA-4−12 demonstrated superwettability, with a water contact angle of 9.5 ± 3.5° in air and an underwater−oil contact angle above 140°, achieving a separation efficiency of 98.5% and a water permeation flux of 2350 L·m^{-2}·h^{-1} for *n*-heptane/water mixtures. The membrane FeOOH@CS/PVA-24−24 exhibited exceptional oil-in-water emulsion separation performance with a separation efficiency of up to 99.9% for water/*n*-heptane emulsions. Additionally, the membrane exhibited remarkable antifouling properties, attributed to its superwetting surface and the photocatalytic ability of β-FeOOH nanoparticles. After five photocatalytic self-cleaning cycles, the water permeation flux and separation efficiency remained almost unchanged, demonstrating its great potential for practical application.

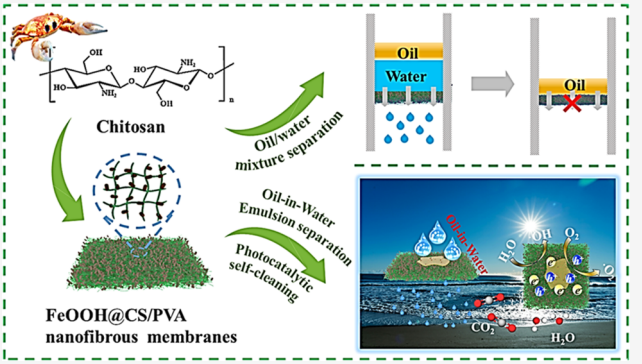

INTRODUCTION

Currently, membrane materials with special wettability have become one of the most effective methods for oily wastewater purification due to their simple process, low cost, high separation efficiency, and excellent selectivity for oil/water mixtures.[1,2] Among these materials, superhydrophilic/underwater oleophobic membranes are gaining substantial focus for their exceptional oil-in-water emulsion separation efficiency and antifouling performance.[3−7] In recent years, the superhydrophilic/underwater oleophobic membrane has been developed normally by introducing a hydrophilic polymer[8,9] containing polar groups such as carboxyl, hydroxyl, and amino groups, etc. onto the surface of substrates, e.g., poly(vinylidene fluoride) (PVDF),[10,11] metal meshes,[12] and nylon membranes,[13,14] through various modification strategies including coating,[1] deposition,[12] grafting,[15,16] etc. Chitosan (CS) is considered one of the commonly used hydrophilic biopolymers for the hydrophilic modification of superwettability membranes/meshes because of its good hydrophilicity, biocompatibility, and biodegradability.[17−19] For instance, Feng et al.[20] developed a superhydrophilic chitosan-tripolyphosphate nanoparticle-modified nylon membrane using a deposition method, which effectively separated oil-in-water emulsions with varying mean particle sizes ranging between 50.9 and 1832.0 nm. However, the aforesaid strategies have inevitable drawbacks, such as inhomogeneous coating and insufficient interfacial strength between the coated layer and the supporting substrates. These issues negatively affect the separation selectivity and wettability of the membrane.[3,21−23] Therefore, developing an inherently hydrophilic and freestanding biobased oil/water separation membrane without the polymeric coating or deposition through a simple process would hold significant application potential for oil/water separation.

Electrospinning technology is a technique for generating nanofibers by applying high-voltage electrostatic force to stretch a viscous polymer solution.[24−26] It possesses powerful structural tunability, enabling the fabrication of porous

Received: October 3, 2024
Revised: December 22, 2024
Accepted: December 23, 2024
Published: December 30, 2024

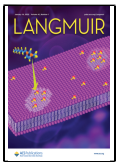

https://doi.org/10.1021/acs.langmuir.4c03882
Langmuir 2025, 41, 633−645

nanofibrous membranes with fiber diameters ranging from tens of nanometers to several micrometers through simple adjustments in composition and appropriate processing optimization. The nanofibrous membranes produced by this technique, with their multilayer micro/nanostructures, high specific surface area, and interconnected porous structure, exhibit high efficiency in treating oily wastewater.[27] Additionally, a freestanding CS-based membrane obtained through electrospinning successfully mitigates the issues related to inadequate interlayer adhesion and uneven coating.[28,29] However, CS itself demonstrates poor spinnability due to the strong intermolecular and intramolecular hydrogen bonds and the bad solubility in most organic solvents.[25,30,31] Since the hydrophilic and eco-friendly poly(vinyl alcohol) (PVA) possesses high spinnability so that it has been used to blend with other polymer solutions such as collagen, gelatin, and alginate to fabricate electrospun membranes.[32,33] Herein, mixing a certain amount of PVA in the CS to prepare the CS/PVA composite electrospinning-used precursor solution is expected to effectively improve the CS's spinnability. Apart from solving the problem of the polymer solution's spinnability, the usage stability of the electrospun membranes is another crucial issue, particularly during the separation of oil/water mixtures.[34−36] For the specific CS/PVA nanofibrous membrane, the inherent hydrophilicity of CS and PVA and the good water solubility feature of PVA make the CS/PVA membrane easy to swell and even partially dissolve when being exposed to the aqueous environment, thus severely limiting their application in oil/water separation.[37] Herein, a post-cross-linking strategy by using the highly active and effective cross-linking agent glutaraldehyde (GA) to further form a stable chemically cross-linked network structure in the membrane is proposed to address the above-mentioned issue. Furthermore, excellent antioil-fouling performance is crucial for the lifespan of membrane materials, which can be enhanced by the synergy of both the hydration mechanism and equipped self-cleaning ability via the photocatalytic oxidation degradation process.[38−40] The hydrophilic β-FeOOH as an active and efficient heterogeneous photocatalyst is therefore considered the potential candidate.[41,42] The $FeCl_3$ solution can act as a precursor, providing iron ions (Fe^{3+}) required for the formation of β-FeOOH. When the CS/PVA membrane is immersed in the $FeCl_3$ solution, the abundant amino and hydroxyl groups on the membrane surface provide sufficient binding sites for anchoring the transition metal cations (Fe^{3+}), resulting in the formation of β-FeOOH nanorod layers.[43] On the one hand, β-FeOOH can effectively degrade oil pollutants through photo-Fenton reactions;[41] on the other hand, the formation of nanoscale rough structures on the hydrophilic membrane surface plays a significant role in regulating the wettability to achieve the superhydrophilicity.[44] Superhydrophilic surfaces can effectively prevent the spreading of oil droplets on their surface through hydration mechanisms, significantly reducing the contact of membrane with oil and further enhancing the antifouling performance.[45,46]

Herein, this study aimed to develop a biobased composite FeOOH@CS/PVA nanofibrous membrane, for oil/water mixture separation by using CS and PVA as precursors through an electrospinning and post-cross-linking strategy, followed by the in situ growth of β-FeOOH on the CS/PVA membrane surface. The coordination of hydroxyl and amino groups of the CS/PVA membrane surface with Fe^{3+} effectively ensures the immobilization of β-FeOOH nanoparticles.[43,44] Specifically, the influences of post-cross-linking time and in situ growth time of β-FeOOH on the membrane's surface morphology and surface wettability were investigated, targeting to extend the application scenario range by effectively separating various types of immiscible oil/water mixtures and oil-in-water emulsions in both mild and harsh aqueous conditions including the acidic, alkaline, and high-salinity environment. Furthermore, the FeOOH@CS/PVA membrane with both post-cross-linking treatment and β-FeOOH in situ growth for 24 h was chosen to assess its photocatalytic self-cleaning performance, demonstrating its potential for oily wastewater treatment.

EXPERIMENTAL SECTION

Materials. Chitosan (low viscosity, <200 mPa·s), poly(vinyl alcohol) (PVA) (1788, degree of alcoholysis 87.0−89.0%), glutaraldehyde (GA, 25 wt %), glacial acetic acid, hydrogen peroxide (H_2O_2, 30%), *n*-heptane, petroleum ether, *n*-hexane, methylene blue, rhodamine B, and Sudan II were purchased from Aladdin Industrial Co. Ltd., Shanghai. Ethanol absolute, anhydrous ferric chloride ($FeCl_3$), sodium hydroxide (NaOH), hydrochloric acid (HCl, 35−37%), methyl orange, and *n*-octane were provided by Sinopharm Chemical Reagent Co., Ltd. Silicone oil and Tween-80 were purchased from Macklin Biochemical Co. Ltd., Shanghai. #100 vacuum pump oil was purchased from Zhuoju Trading Co., Ltd., Shanghai. Silver nitrate was purchased from West Asia Chemical Technology Co. Ltd., Shandong. Vegetable oil was supplied by the local market. All chemicals were used as received.

Preparation of CS/PVA Nanofibrous Membranes. A precursor solution for electrospinning was prepared by mixing an 8 wt % PVA aqueous solution with a 2 wt % CS solution (dissolved in 90 wt % glacial acetic acid) in a mass ratio of 7:3. The electrospinning experiments utilized this precursor solution under specific conditions, which included a voltage of 17 kV, a feed rate of 0.005 mL/min, a distance of 15 cm between the collector and the needle, a chamber temperature of 25 °C, and a relative humidity level of 20%. After electrospinning for 12 h, the obtained membrane was placed in a vacuum drying oven at 60 °C for 24 h to remove the remaining solvents. The dried membrane was subsequently immersed in a 2 wt % glutaraldehyde (GA) solution (ethanol solvent) for cross-linking treatment at 37 °C for 4 and 24 h to obtain CS/PVA nanofibrous membranes. The prepared CS/PVA membranes were labeled as CS/PVA-*X*, where *X* represents the cross-linking time (h).

Preparation of FeOOH@CS/PVA Nanofibrous Membranes. The CS/PVA nanofibrous membranes are immersed in a 12 mg/mL $FeCl_3$ solution, with temperature being maintained at 60 °C, for controlled soaking durations of 12 and 24 h to facilitate the in situ growth of β-FeOOH nanoparticles. Subsequently, the membranes were immersed in water for 12 h to remove surface physical accumulations of impurities, followed by drying at room temperature to obtain the final FeOOH@CS/PVA nanofibrous membranes. The as-prepared FeOOH@CS/PVA nanofibrous membranes were denoted as FeOOH@CS/PVA-*X*-*Y*, where *Y* represents the in situ growth time of β-FeOOH nanoparticles.

Characterization Methods. The microstructures and surface morphologies of both CS/PVA membranes and FeOOH@CS/PVA membranes were analyzed utilizing an ultrahigh-resolution field emission scanning electron microscope (FE-SEM, Hitachi S-4800). Samples were sputter-coated with 4 nm-thick gold layers before SEM observation. The pore size of the membrane samples and the particle size of β-FeOOH nanoparticles on the membrane surface are measured using ImageJ software with at least 200 measurements taken for each sample. For FeOOH nanoparticles, the length of each particle's major and minor axes was measured with the overall average size. Fourier transform infrared spectroscopy (FT-IR, Thermo-Fisher Nicolet iS5) was applied at a resolution of 4 cm^{-1} in a range of 4000−500 cm^{-1} to analyze the functional groups of the membranes. The crystal structures of the membranes were evaluated via an X-ray

https://doi.org/10.1021/acs.langmuir.4c03882
Langmuir 2025, 41, 633−645

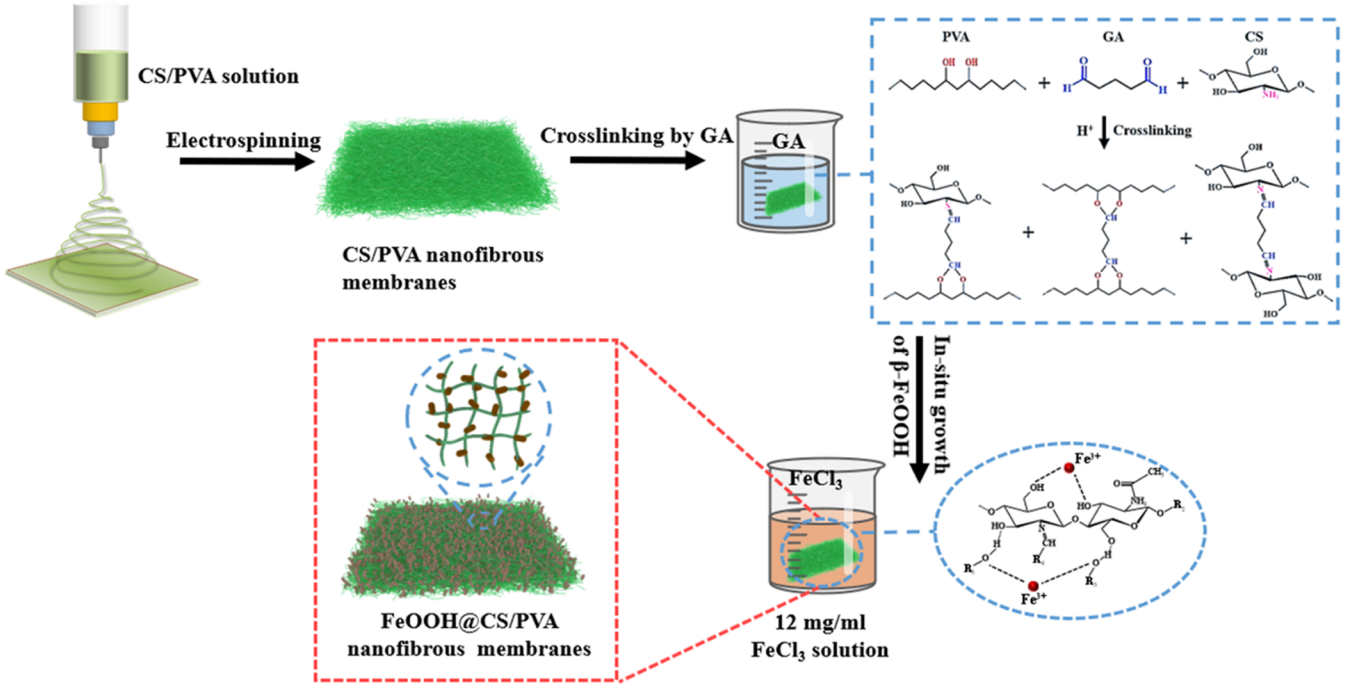

Figure 1. Schematic illustration showing the fabrication process of the FeOOH@CS/PVA nanofibrous membranes.

diffractometer (XRD, PANalytical B.V. X'Pert PRO MPD) using the Cu Ka radiation (λ = 1.5418 Å, 40 kV, 40 mA) in the range of 10−75° at a scanning rate of 1°·min^{-1}. The wetting properties of the membranes, which encompassed water contact angles (WCAs) and underwater−oil contact angles (UWOCAs), were assessed with a contact angle analyzer (model DSA30, KRUSS) at at least three different positions. The contact angle measurement represented the average of three readings taken at various locations on each sample's surface. The oil content in the filtrates was assessed using a total organic carbon analyzer (Shimadzu, TOC-L).

Immiscible Oil/Water Separation Experiments. Oils such as *n*-heptane, silicone oil, petroleum ether, vegetable oil, and pump oil with water were used to construct immiscible oil/water contaminants, maintaining an oil/water mass ratio of 3:7. To clearly differentiate the oil layer from the water layer, Sudan Red II and methylene blue were used to dye the oil and water, respectively. Before use, the membrane was prewetted with deionized water and secured between two glass cylinder tubes with a diameter of 15 mm each. Subsequently, 10 mL of immiscible oil/water mixture underwent oil/water separation, allowing the filtered water and nonpermeated oil to be collected separately. The separation efficiency (η) was calculated using eq 1

$$\eta = \frac{m_1}{m_0} \times 100\% \tag{1}$$

where m_0 (g) represents the mass of water before separation and m_1 (g) denotes the mass of water that has been filtered after the separation.

The water permeation flux (F, L·m^{-2}·h^{-1}·bar^{-1}) was calculated according to eq 2

$$F = \frac{V}{A \times t \times P} \tag{2}$$

where V (L) represents the total volume of filtrate collected, A (m^2) refers to the area which the oil/water mixtures pass through during filtration, t (h) is the time for collecting the filtrate, and P (bar) is the driving pressure. In the process of separating immiscible oil/water mixtures solely by gravity, the driving pressure (P) can be neglected.

Stability of the FeOOH@CS/PVA Nanofibrous Membrane. Neutral-pH deionized water was replaced with 1 M HCl, 1 M NaOH, and 1 M NaCl solutions to simulate acidic, alkaline, and high-salinity environments, respectively. *n*-Heptane was selected as the oil contaminant, and subsequently, the membrane materials were employed to separate *n*-heptane/corrosive solutions using the aforementioned oil/water separation test in order to evaluate the performance of the membrane materials in terms of oil/water separation under extreme conditions.

Emulsion Separation Experiments. For the emulsion system, oil-in-water emulsions with an oil-to-water ratio of 1:9 were prepared using *n*-heptane, *n*-hexane, *n*-octane, and vegetable oil. The mixture was then stirred at 900 rpm for 5 h at 25 °C, followed by ultrasonic treatment for 2 h, resulting in a white milky solution. As shown in Figure S1, the prepared emulsion remained in a stable emulsified state even after being stored at room temperature for 2 h. The oil-in-water emulsion separation study was performed immediately after the emulsion sample was freshly prepared. Herein, the emulsion separation process was conducted under the pressure of 0.05 MPa, with the solution in the upper tube maintained at a stable level. Separation efficiency (η) was calculated using eq 3

$$\eta = \left(1 - \frac{C_1}{C_2}\right) \times 100\% \tag{3}$$

where C_2 and C_1 are the oil content in the emulsions and the filtrates, respectively.

Photocatalytic Self-Cleaning Experiments. The photocatalytic self-cleaning performance of the FeOOH@CS/PVA nanofibrous membrane is evaluated by monitoring the variation in water permeation flux after cyclic separation processes, accompanied by the cleaning step. Specifically, five cycles of separation experiments were conducted with *n*-heptane/pure water emulsions. After each emulsion separation, the membrane contaminated with the oil/water emulsion was placed in a 0.2 vol % H_2O_2 solution and exposed to 300 W visible light for 10 min. Under visible light irradiation, β-FeOOH can react with H_2O_2 in a photo-Fenton reaction to generate hydroxyl radicals with extremely strong oxidative capabilities, which can effectively degrade organic compounds.[47]

Swelling Test. The CS/PVA-4 and CS/PVA-24 membrane samples with the area of 2 cm × 2 cm were immersed in 20 mL of deionized water and kept for 24 h to reach the swelling equilibrium. The swelling degree (SD) of the membrane at equilibrium was calculated according to eq 4

https://doi.org/10.1021/acs.langmuir.4c03882
Langmuir 2025, 41, 633−645

$$SD = \frac{W_1 - W_0}{W_0} \times 100\% \quad (4)$$

where W_0 (g) and W_1 (g) represent the weight of the membrane before and after 24 h of swelling, respectively.

RESULTS AND DISCUSSION

As shown in Figure 1, the CS/PVA nanofibrous membrane was synthesized using chitosan and poly(vinyl alcohol) by an electrospinning strategy and post-cross-linking process. The FeOOH@CS/PVA nanofibrous membrane was further fabricated by in situ growing β-FeOOH nanorods on the CS/PVA nanofibrous membrane's surface.

Due to the intrinsic hydrophilicity of CS and PVA, as well as the water solubility of PVA, the uncross-linked CS/PVA-0 membrane experiences swelling and dissolution in water, leading to the destruction of the membrane structure.[37] To improve the durability of the CS/PVA nanofibrous membrane in the aqueous environment, a three-dimensional (3D) covalent cross-linking network was formed by cross-linking the main components CS and PVA with GA.[48,49] As shown in Figure S2, the uncross-linked CS/PVA-0 dissolved when being immersed in water for 0, 2, and 4 h, while CS/PVA-4 and CS/PVA-24 could retain their structural integrity after 4 h of immersion in water, which gives a hint of successful cross-linking in the samples CS/PVA-4 and CS/PVA-24. After being immersed in the water for 24 h to reach the swelling equilibrium, the SDs of CS/PVA-4 and CS/PVA-24 were calculated to be 5.81 and 3.64, respectively, according to eq 4. The relatively low swelling degrees further confirmed the excellent durability of CS/PVA-4 and CS/PVA-24 in the aqueous environment due to the formed 3D cross-linked network. This was mainly due to the cross-linking reaction between the aldehyde groups in GA and the amino groups ($-NH_2$) of CS and the hydroxyl groups ($-OH$) of PVA when the CS/PVA nanofibrous membrane was immersed in a 2 wt % GA solution (ethanol solvent), forming imine bonds ($-C{=}N-$) and ether bonds ($-C-O-C-$), which leads to the formation of a cross-linked structure and enhances the three-dimensional network of the material (Figure S3).[49] FTIR spectroscopy further confirmed the successful cross-linking of the CS/PVA nanofibrous membrane with GA. As shown in Figure 2, the broad peaks in the 3000−3500 cm^{-1} range represent the stretching vibrations of $-NH_2$ and $-OH$ groups in chitosan and poly(vinyl alcohol) molecules, as well as intermolecular hydrogen bonding. Compared to CS/PVA-0 (black line), the FT-IR spectra of CS/PVA-4 (red line) and CS/PVA-24 (blue line) exhibit peaks at 1710 and 1140 cm^{-1}, attributed to carbonyl groups and C−O−C stretching vibrations, respectively. This confirms that the hydroxyl groups of PVA or CS and the aldehyde groups of GA have undergone a hemiacetal and acetal reaction.[50] The characteristic absorption peak at 1640 cm^{-1} is related to the formation of C═N bonds in imines, confirming the formation of aldehyde-imine linkages between the amino groups of CS and the aldehyde groups of GA.[49,51] These variations of absorption peaks indicated that CS may have cross-linked with PVA through GA, forming a 3D covalent network structure.[52] Further, the lower SD value of CS/PVA-24 compared with that of CS/PVA-4 indicates a higher degree of cross-linking in CS/PVA-24. This can also be verified by their FTIR spectra (Figure 2). As the cross-linking time increases, the absorption intensities of the C−O−C stretching vibrations and the C═N stretching vibration of imine groups are significantly enhanced, suggesting a higher degree of cross-linking in CS/PVA-24.

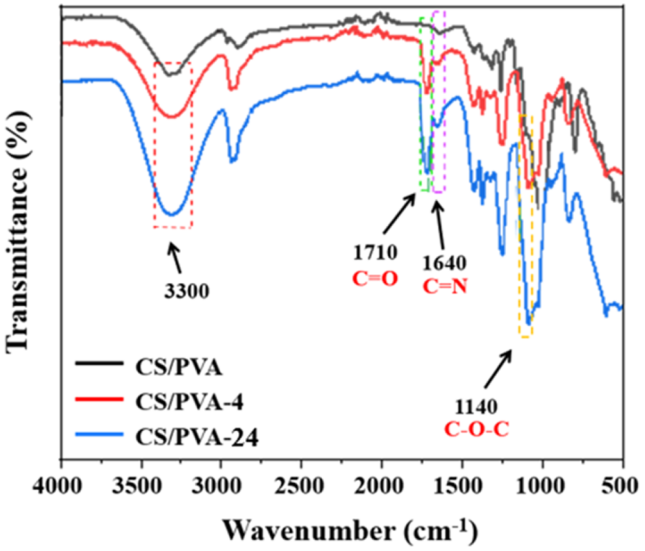

Figure 2. FT-IR spectra of the membranes with different post-cross-linking times of 0, 4, and 24 h.

The morphologies of CS/PVA-0, CS/PVA-4, and CS/PVA-24 were characterized by SEM. As shown in Figure 3a, the uncross-linked CS/PVA-0 nanofibrous membrane exhibited a network structure composed of woven nanofibers. There is no adhesion or entanglement between the neighboring nanofibers. In comparison, as shown in Figure 3b,c, after the post-cross-linking process, the membranes CS/PVA-4 and CS/PVA-24 demonstrated porous network structures with some fibers merging together.[53] Specifically, extension of the cross-linking time caused a larger number of fibers to merge. Accordingly, the membrane pore size was significantly reduced from 0.93 ± 0.22 to 0.45 ± 0.10 μm (Figure 3d,f). The structural transformation should be related with the cross-linking reaction of GA with CS and PVA, which is also consistent with the FT-IR spectral results.

The surface wettability of CS/PVA-4 and CS/PVA-24 was further evaluated through water contact angle (WCA) measurements. As illustrated in Figure 4a,b, all the prepared membranes demonstrated a hydrophilic surface, but increasing the cross-linking time from 4 to 24 h led to the increase of the WCA from 34.3 ± 3.2 to 39.8 ± 2.5°, indicating the decrease in hydrophilicity, which should be ascribed to the consumption of hydrophilic amino and hydroxyl groups of CS and PVA during the cross-linking process.[54] Since better hydrophilicity favors the selectivity of oil/water mixtures,[55] applying 4 h of post-cross-linking treatment was rational for the oil/water separation application and CS/PVA-4 was considered the potential candidate for further investigation. As shown in Figure 4c, the underwater−oil contact angles (UWOCAs) of CS/PVA-4 were measured to be 127.1 ± 3.3, 132.5 ± 2.6, 135.2 ± 3.2, and 132.1 ± 2.9°, respectively, for all four types of oil droplet including *n*-heptane, *n*-hexane, petroleum ether, and vegetable oil, indicating good underwater oleophobic performance.

The FeOOH@CS/PVA nanofibrous membrane was further fabricated by in situ growing β-FeOOH on the CS/PVA nanofibrous membrane's surface. Figure 5a shows the schematic diagram of the in situ growth mechanism of β-FeOOH. When the CS/PVA membrane is immersed in the

https://doi.org/10.1021/acs.langmuir.4c03882
Langmuir 2025, 41, 633−645

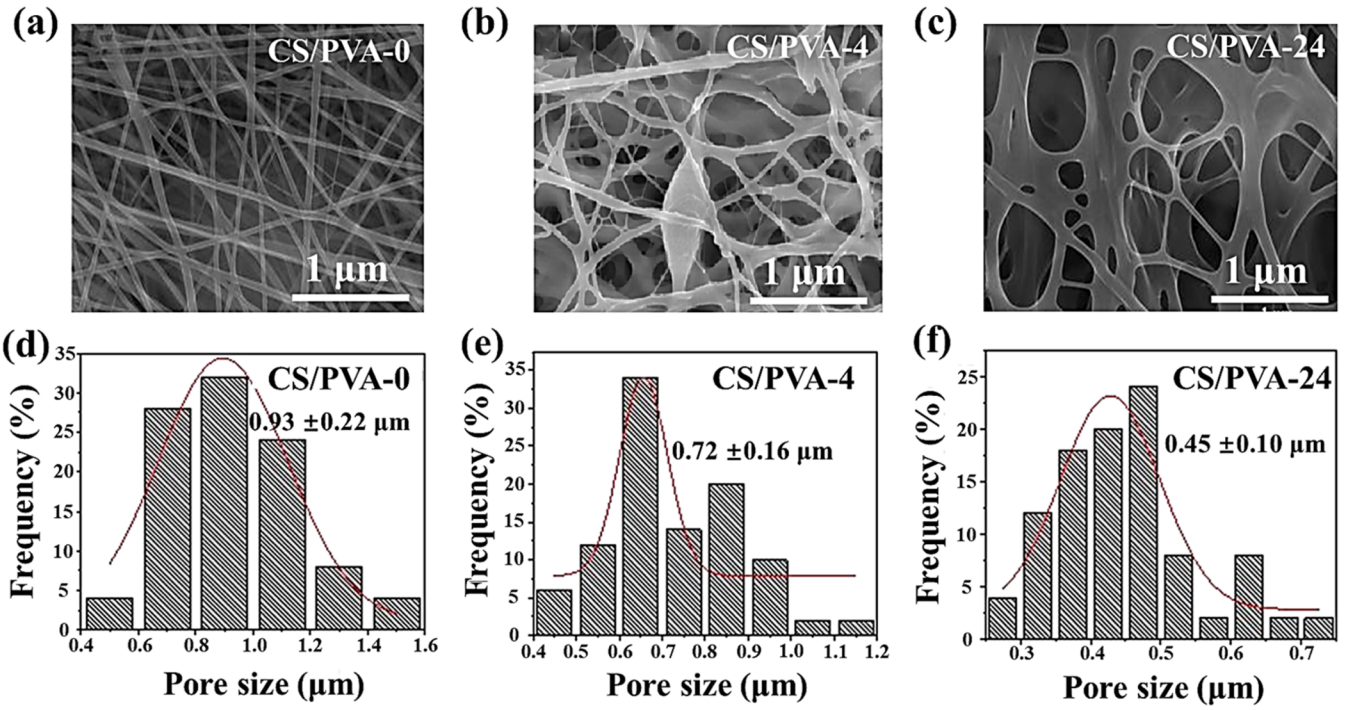

Figure 3. (a–c) SEM images and (d–f) pore size distribution statistics of CS/PVA nanofibrous membranes at different post-cross-linking times of 0, 4, and 24 h.

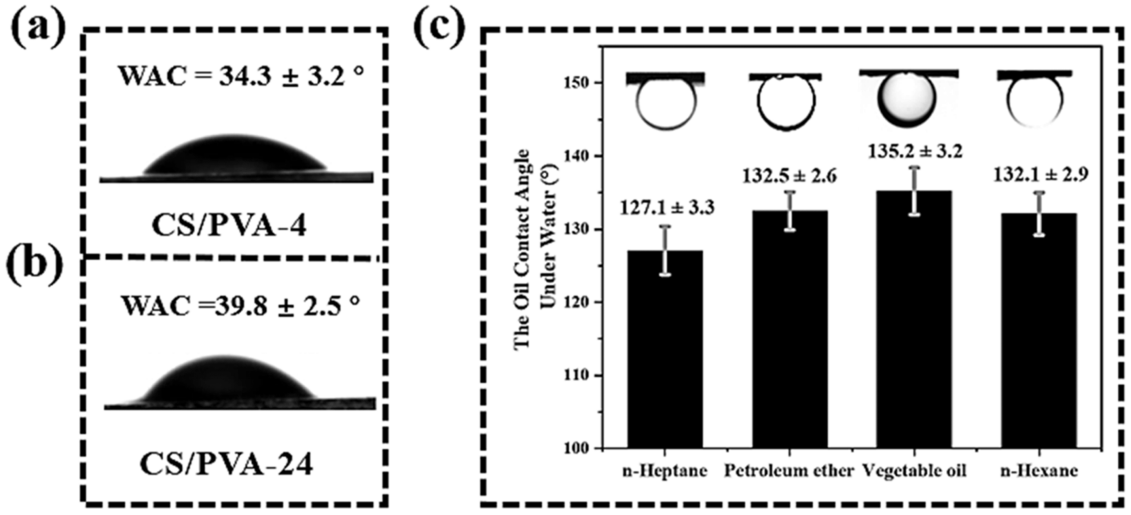

Figure 4. Water contact angles of (a) CS/PVA-4 and (b) CS/PVA-24. (c) Oil contact angles underwater of CS/PVA-4 measured with various oil types.

$FeCl_3$ solution, the plentiful hydroxyl and amino groups in the CS/PVA nanofibrous provide sufficient sites for the coordination of Fe^{3+}. Fe^{3+} can coordinate with the electron-rich oxygen atoms of the polar hydroxyl groups. Also, the nitrogen atom in the amino group can also coordinate with Fe^{3+} through its lone pair of electrons. The anchored Fe^{3+} subsequently undergo hydrolyzed in the solution, forming $Fe(OH)_3$, which accumulates on the surface of the CS/PVA nanofibrous membrane. At 60 °C, the precipitated $Fe(OH)_3$ can undergo further dehydration and reorganization of iron and oxygen atoms, leading to the formation of a more stable hydroxide–oxide iron structure (β-FeOOH).[56,57] To achieve the effective separation of different types of oily wastewater, three FeOOH@CS/PVA membranes with difference in the pore structures were prepared by adjusting the cross-linking time and the in situ growth time of β-FeOOH nanoparticles. These membranes are designated as FeOOH@CS/PVA-4–12, FeOOH@CS/PVA-4–24, and FeOOH@CS/PVA-24–24.

As shown in Figure 5b, for all the samples, the peak appearing at 657 cm^{-1} in the FT-IR spectra of all three membrane materials corresponds to the stretching or lattice vibration of the Fe–O bond, indicating that β-FeOOH nanoparticles grew on the surface of the membranes.[58] By comparing the FT-IR spectra of FeOOH@CS/PVA-4–12 and FeOOH@CS/PVA-4–24, it is evident that the Fe–O bond peak intensity of FeOOH@CS/PVA-4–24 is stronger, which should be attributed to an increase in the number and particle size of β-FeOOH nanoparticles with a longer period of in situ

https://doi.org/10.1021/acs.langmuir.4c03882
Langmuir 2025, 41, 633–645

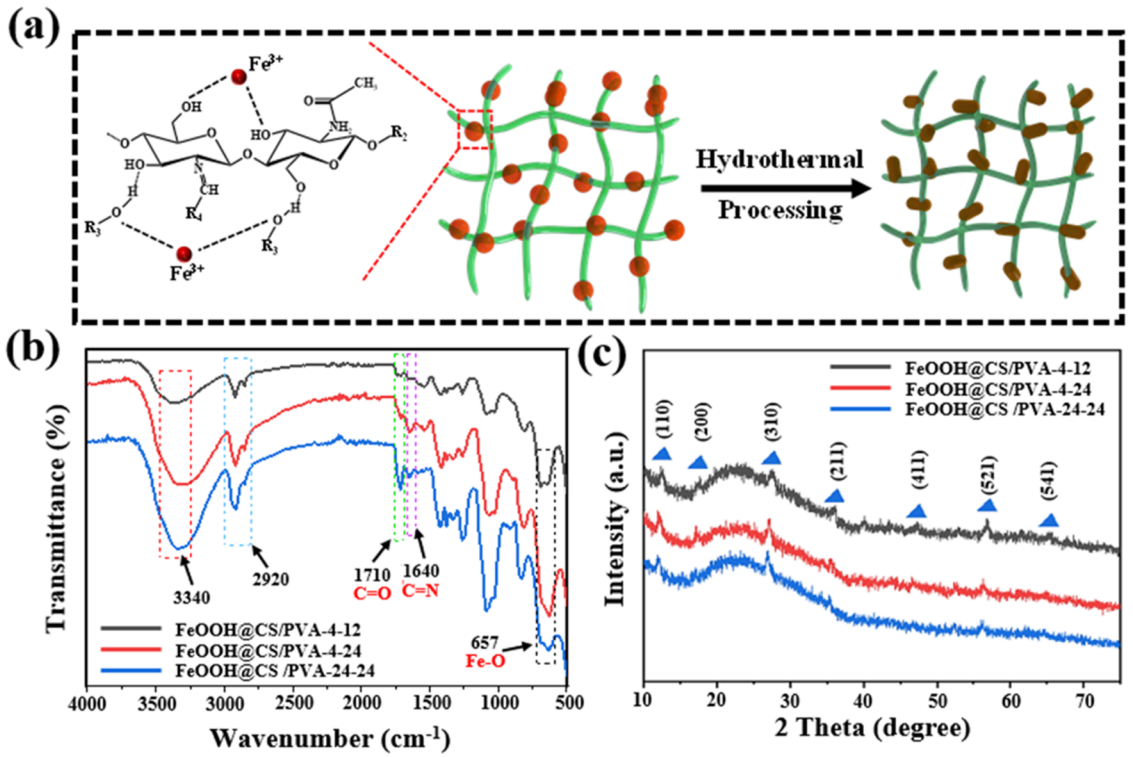

Figure 5. (a) Schematic diagram showing the in situ growth mechanism of β-FeOOH. (b) FT-IR spectra and (c) XRD patterns of FeOOH@CS/PVA-4−12, FeOOH@CS/PVA-4−24, and FeOOH @CS/PVA-24−24.

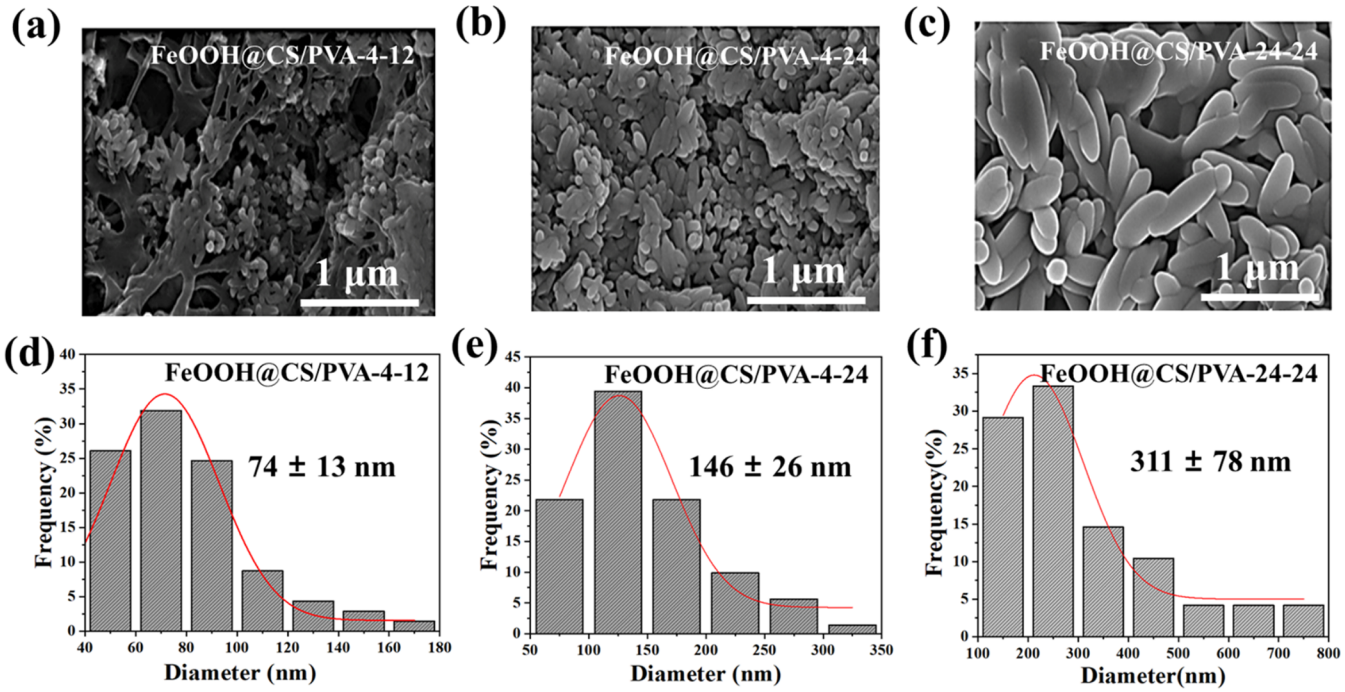

Figure 6. SEM images of (a) FeOOH @CS/PVA-4−12, (b) FeOOH @CS/PVA-4−24, and (c) FeOOH @CS/PVA-24−24. The particle size statistics of β-FeOOH grown on the surface of (d) FeOOH@CS/PVA4−12, (e) FeOOH@CS/PVA-4−24, and (f) FeOOH@CS/PVA-24−24.

growing time. The crystalline phase structure of the membranes was analyzed by XRD. As shown in Figure 5c, for all these three membranes, after the in situ growth process, the typical diffraction peaks belonging to β-FeOOH at 2θ = 11.7, 16.7, 26.6, 35.3, 46.6, 55.8, and 64.1°show up, corresponding to the (110), (200), (310), (211), (411), (521), and (541) crystalline planes, respectively,[59] thus further proving the successful growth of β-FeOOH nanoparticles on the membrane surface.

The surface morphologies of FeOOH@CS/PVA-4−12, FeOOH@CS/PVA-4−24, and FeOOH@CS/PVA-24−24 nanofibrous membranes were characterized by SEM, and the size distribution of the formed β-FeOOH particles was counted accordingly. As shown in Figure 6a−c, compared to

https://doi.org/10.1021/acs.langmuir.4c03882
Langmuir 2025, 41, 633−645

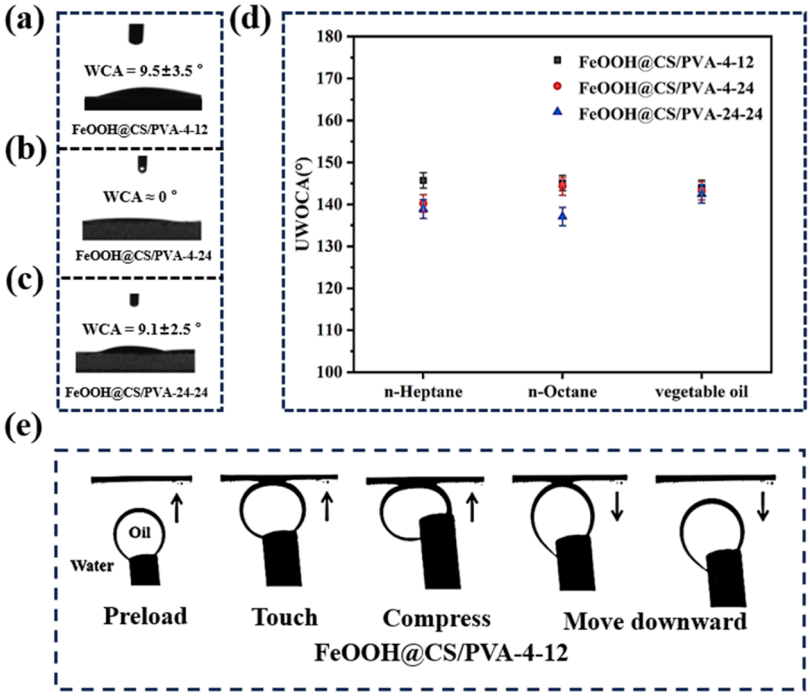

Figure 7. Water contact angle of (a) FeOOH@CS/PVA-4−12, (b) FeOOH@CS/PVA-4−24, and (c) FeOOH @CS/PVA-24−24 in air. (d) Underwater−oil contact angles of FeOOH@CS/PVA-4−12, FeOOH@CS/PVA-4−24, and FeOOH@CS/PVA-24−24 were measured for different oil pollutants, including *n*-heptane, *n*-octane, and vegetable oil. (e) Dynamic adhesion test of the *n*-heptane oil droplet underwater was conducted on the FeOOH@CS/PVA-4−12 membrane.

the smooth surface of the CS/PVA nanofibrous membrane, the FeOOH@CS/PVA nanofibrous membrane exhibited distinct nanorod layers on its surface, demonstrating the successful introduction of β-FeOOH particles to the CS/PVA nanofibrous membrane. Specifically, as shown in Figure 6a,b, extending the in situ growth time results in β-FeOOH nanorods with a more uniform distribution and larger size.[60] Accordingly, the particle size of β-FeOOH significantly increased from 74 ± 13 to 146 ± 26 μm (Figure 6d,e). It is noticeable that the β-FeOOH nanoparticle size of the FeOOH@CS/PVA-24−24 membrane was measured to be 311 ± 78 nm, which is significantly greater than that on the FeOOH@CS/PVA-4−24 membrane (Figure 6e,f); this might be attributed to the longer cross-linking time of the CS/PVA-24, leading to smaller pore size of 0.45 ± 0.10 μm (shown in Figure 3e), which is more beneficial for the loading of β-FeOOH nanoparticles.[61] Additionally, the pore size of the FeOOH@CS/PVA nanofibrous membrane can be adjusted by controlling the in situ growth time of β-FeOOH. As shown in Figures S4c and 3e, with the increase in the quantity and size of β-FeOOH nanoparticles, the pore size of the membrane was significantly reduced from 0.45 ± 0.10 to 0.12 ± 0.03 μm.

To figure out the influence of β-FeOOH on the membrane's wettability, the WCAs of the FeOOH@CS/PVA-4−12, FeOOH@CS/PVA-4−24, and FeOOH@CS/PVA-24−24 were measured. As shown in Figure 7a,b, the WCA of FeOOH@CS/PVA-4−12 in air was 9.5 ± 3.5°, significantly lower than the 34.3 ± 3.2° of CS/PVA-4, indicating that the membrane changed its wettability from hydrophilic to superhydrophilic with the incorporation of β-FeOOH. This can be attributed to the improved surface roughness of the membrane introduced by the nanoscale β-FeOOH particles.[59,62] In comparison, with the increasing growth time of β-FeOOH from 4 to 24 h, the FeOOH@CS/PVA-4−24 demonstrated a WCA of nearly 0°, possibly due to the complete growth of nanometer-sized β-FeOOH on the membrane surface, which further increased the surface roughness (Figure 6a,b). The WCA of FeOOH@CS/PVA-24−24 was measured to be 9.1 ± 2.5°, which is higher than that of FeOOH@CS/PVA-4−24 (Figure 7c), indicating the decreased hydrophilicity, which should be attributed to the larger number of consumed hydroxyl and amino groups with the extension of the post-cross-linking process. Further, the underwater−oil contact angles of the above-fabricated membranes FeOOH@CS/PVA-4−12, FeOOH@CS/PVA-4−24, and FeOOH@CS/PVA-24−24 were investigated. As shown in Figure 7d, the UWOCAs of these three membranes toward *n*-heptane, *n*-octane, and vegetable oil were all above 140°, indicating their excellent underwater oleophobic properties, which could bring potential antioil-fouling performance.[63] The underwater dynamic oil adhesion study of the membrane with FeOOH@CS/PVA-4−12 as the demo can reflect the membranes' antifouling performance to some extent. Figure 7e illustrates that after the needle tip, preloaded with a 2 μL *n*-heptane oil droplet, made contact with and then departed from the surface of the FeOOH@CS/PVA-4−12 membrane underwater, the *n*-heptane droplet was completely detached from the membrane surface without any residues left, thus demonstrating that FeOOH@CS/PVA-4−12 had an ultralow oil adhesion performance underwater. Since FeOOH@CS/PVA-4−24 possessed the lowest WCA and FeOOH@CS/PVA-24−24 possessed a similar WCA as FeOOH@CS/PVA-4−12, it can be inferred that apart from FeOOH@CS/PVA-4−12, FeOOH@CS/PVA-4−24 and FeOOH@CS/PVA-24−24 should also have ultralow oil adhesion property.

The superhydrophilic and underwater oleophobic characteristics observed in the membrane samples could lead to outstanding performance in oil/water separation. Therefore,

https://doi.org/10.1021/acs.langmuir.4c03882
Langmuir 2025, 41, 633−645

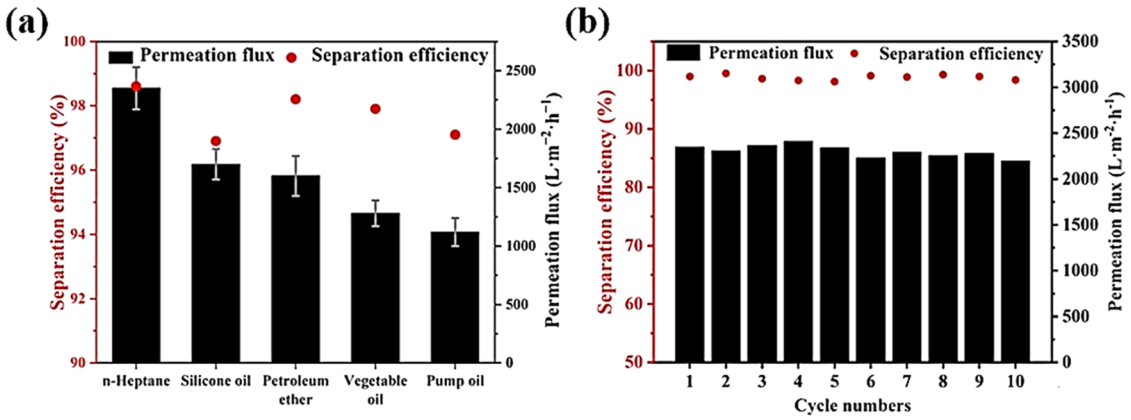

Figure 8. (a) Separation efficiency and water permeation flux of FeOOH@CS/PVA-4−12 nanofibrous membranes toward various oil/water mixtures. (b) Water permeation flux and separation efficiency of the membrane FeOOH@CS/PVA-4−12 during the 10-time cyclic *n*-heptane/water mixture separation test.

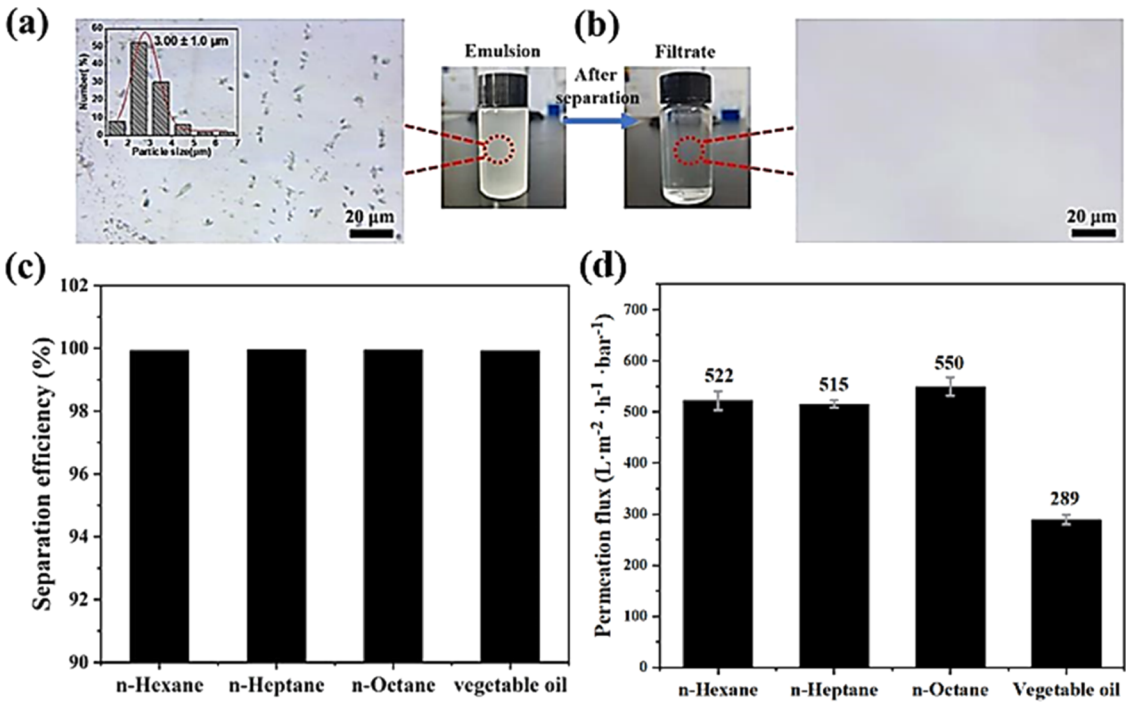

Figure 9. Optical micrographs and photos showing the *n*-heptane-in-water emulsions (a) before and (b) after separation. (c) Separation efficiency and (d) water permeation flux of FeOOH@CS/PVA-24−24 toward various oil-in-water emulsions.

various oil/water mixtures (including *n*-heptane, silicone oil, petroleum ether, vegetable oil, and pump oil) were prepared and filtered through a gravity-driven separation device embedded with an FeOOH@CS/PVA-4−12 membrane. The separation efficiency (η) and water permeation flux (F) were calculated according to eqs 1 and 2, respectively. As shown in Figure 8a, the FeOOH@CS/PVA-4−12 nanofibrous membrane achieved a separation efficiency of over 97.0% toward all five types of oil/water mixtures, thus indicating wide effectiveness toward different oil contaminants. The water permeation fluxes for the targeted oil/water mixtures ranged from 1120 to 2350 $L{\cdot}m^{-2}{\cdot}h^{-1}$, despite being influenced largely by the oil viscosity, still remaining at a relatively high level. Notably, the separation efficiency of FeOOH@CS/PVA-4−12 toward the *n*-heptane/water mixture reached 98.5%, with a water permeation flux of 2350 $L{\cdot}m^{-2}{\cdot}h^{-1}$, both of which are higher than some previous related studies.[64−66] Subsequently, a cyclic separation test involving *n*-heptane/water was conducted 10 times to further examine the operational stability of the FeOOH@CS/PVA-4−12 membrane. As shown in Figure 8b, after ten cycles of separation, the separation efficiency toward *n*-heptane/water still exceeded 97.3% and the water permeation flux was 2240 $L{\cdot}m^{-2}{\cdot}h^{-1}$, confirming its stable and durable separation performance. These results highlight the highly efficient oil/water separation performance of the membranes in a wide range.

Achieving effective and reliable oil/water separation performance in challenging aqueous environments is of paramount importance for practical application.[67] Therefore, the membrane FeOOH@CS/PVA-4−12 was assessed for its separation efficiency in the *n*-heptane/water mixture under the acidic, alkaline, or saline conditions. As shown in Figure S5a, the *n*-heptane phase dyed orange by Sudan II was all intercepted by the upper surface of the membrane, whereas

https://doi.org/10.1021/acs.langmuir.4c03882
Langmuir 2025, 41, 633−645

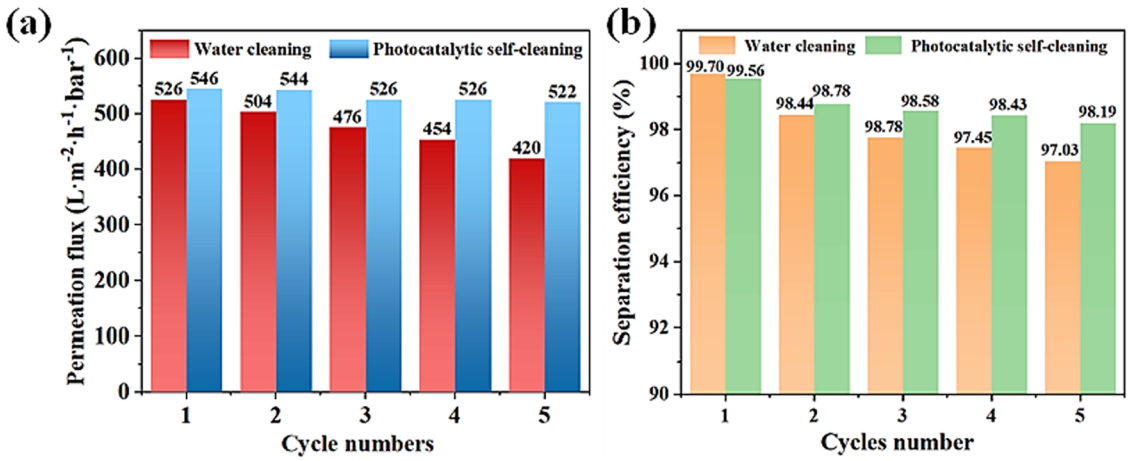

Figure 10. (a) Water permeation fluxes and (b) separation efficiency of FeOOH@CS/PVA-24−24 in the cyclic separation test of *n*-heptane/pure water emulsion using either conventional water cleaning or the photocatalytic self-cleaning method.

the water phase containing 1 M HCl, NaOH, or NaCl passed through the membrane with evidence from the changed color of the pH strip or formed milky white AgCl flocculent in the beaker. As shown in Figure S5b,c, the separation efficiencies and the water permeation fluxes of FeOOH@CS/PVA-4−12 under the above three harsh conditions remained above 98.5% and 2500 $L{\cdot}m^{-2}{\cdot}h^{-1}$, which did not show much difference compared with the results obtained from separating the heptane/neutral-pH water mixture, indicating that the fabricated membrane has superior chemical stability. Such favorable performance should correspond to the stable porous network structure due to the chemical cross-linking function of GA. Also, the in situ growth strategy ensured the robust anchoring of β-FeOOH nanoparticles on the membrane surface due to the strong coordination interaction between Fe^{3+} and the amino and hydroxyl groups of the CS/PVA membrane.

Compared to the immiscible oil/water mixture separation, separating oil/water emulsions is more challenging since the emulsified oil droplet normally has smaller sizes of less than 20 μm, which requires the membrane to have more elaborate design with finer apertures and a superior superwetting surface.[68] The membrane FeOOH@CS/PVA-24−24 was selected for the oil-in-water emulsion study considering its superhydrophilicity and the smallest aperture of 0.12 ± 0.03 μm compared with that of FeOOH@CS/PVA-4−12 and FeOOH@CS/PVA-4−24 due to the synergistic effect of the intensified cross-linking degree and long in situ growth time of β-FeOOH (Figure S4).[53] The optical micrographs and photos of the emulsified *n*-heptane/water mixture illustrated in Figure 9a,b clearly demonstrated that after separation by the membrane FeOOH@CS/PVA-24−24, the initial opaque *n*-heptane/water emulsion with the *n*-heptane droplet average size of around 3.0 ± 1.0 μm became transparent, and there is no visible oil droplet discovered in the optical micrograph, proving the effective oil-in-water emulsion separation performance of the membrane FeOOH@CS/PVA-24−24. Further, a wider scope of emulsified oil/water mixtures including *n*-hexane, *n*-octane, and vegetable oil were tested to investigate the membrane's universal application. The water permeation flux (F) and separation efficiency (η) of the FeOOH@CS/PVA-24−24 membrane for the oil-in-water emulsions were calculated according to eqs 2 and 3. As shown in Figure 9c,d, FeOOH@CS/PVA-24−24 demonstrated superior separation efficiencies of over 99.9% for all tested oil-in-water emulsions with the corresponding permeation fluxes of 522, 515, 550, and 289 $L{\cdot}h^{-1}{\cdot}m^{-2}{\cdot}bar^{-1}$, respectively. This study compares the performance of FeOOH@CS/PVA nanofibrous membranes with similar materials and technologies reported in the existing literature, as shown in Table S1.[19−21,69−72] The results indicate that, compared to previous reports, the FeOOH@CS/PVA nanofibrous membranes exhibit comparable separation performance. Furthermore, most membranes are only effective in separating immiscible oil/water mixtures but are unable to separate oil/water emulsions. Some membranes, although capable of separating oil/water emulsions, often face lower water permeation flux when separating immiscible oil/water mixtures. As a result, a single membrane typically cannot achieve effective separation of both immiscible oil/water mixtures and oil/water emulsions simultaneously. This study enables precise control of the pore size of FeOOH@CS/PVA nanofibrous membranes by simply adjusting the preparation process parameters and thus can effectively separate both immiscible oil/water mixtures and oil/water emulsions. After the separation process of *n*-hexane/water, *n*-heptane/water, *n*-octane/water, and vegetable oil/water emulsions, the total organic carbon (TOC) content in the water phase was significantly low, measured to be 5.5, 8.0, 15.5, and 28.0 $mg{\cdot}L^{-1}$, respectively (Figure S6), which were all below 30 $mg{\cdot}L^{-1}$, thus meeting the treatment standards for urban wastewater as specified by most countries around the world,[73,74] further confirming that the as-fabricated FeOOH@CS/PVA-24−24 exhibits high oil/water separation efficiency.

Imparting good photocatalytic self-cleaning ability to the FeOOH@CS/PVA membrane is expected to enhance its antioil-fouling performance,[38,75] which can be evaluated by monitoring changes in the water permeation flux and separation efficiency during the cyclic separation process, followed by the cleaning step. To explore this, two groups of five-cycle *n*-heptane/pure water emulsion separation studies were carried out. Group A was cleaned by immersing them in a 0.2 vol % H_2O_2 solution and under 300 W visible light, whereas the membranes in Group B were cleaned by immersing in deionized water without light exposure. As shown in Figure 10a,b, the water permeation flux of the membranes in Group B only slightly decreased from the initial value of 526 to 420 $L{\cdot}m^{-2}{\cdot}h^{-1}{\cdot}bar^{-1}$ and the separation efficiency only decreased from 99.7 to 97.3%. This is due to β-

https://doi.org/10.1021/acs.langmuir.4c03882
Langmuir 2025, 41, 633−645

FeOOH creating a nanoscale rough structure on the hydrophilic membrane surface, which endows the membrane with superhydrophilicity and consequently good antioil-fouling performance. It is also noticeable for Group A, which was applied with the photocatalytic self-cleaning method; when comparing the fifth and the first cycle, the water permeation flux difference was even smaller, only dropping from 546 to 522 $L{\cdot}m^{-2}{\cdot}h^{-1}{\cdot}bar^{-1}$. Also, within these five cycles, the water permeation fluxes of Group A were all higher than those of Group B. Furthermore, after five cycles, the membrane still retained a high separation efficiency of 98.19%, which can be attributed to the presence of β-FeOOH nanoparticles imparting an excellent photocatalytic self-cleaning performance to the FeOOH@CS/PVA nanofibrous membranes. The cause of this phenomenon is likely linked to the photocatalytic properties of β-FeOOH nanoparticles. As showed in Figure S7, when exposed to visible light irradiation, these nanoparticles produce a significant number of electron−hole pairs, which catalyze the conversion of hydrogen peroxide into a large quantity of hydroxyl radicals ($^{\bullet}OH$). The oxidative capacity of $^{\bullet}OH$ enables the degradation of various organic pollutants on the membrane surface into smaller entities, such as CO_2 and H_2O, through redox reactions. This process effectively removes persistent pollutants from the membrane surface,[40,41] presenting a promising approach to improve both the durability and efficiency of oil/water separation membranes.

CONCLUSIONS

In summary, the biobased superwetting composite nanofibrous membranes used for oil/water separation are electrospun with hydrophilic CS and PVA as precursors, followed by chemical cross-linking and in situ growth of β-FeOOH nanoparticles on the surface. By precisely controlling the cross-linking time between CS and PVA, as well as the growth time of β-FeOOH nanoparticles, nanofibrous membranes with the variation in the pore size were fabricated to optimize the separation of floating oil/water systems and oil/water emulsions. Moreover, the presence of β-FeOOH nanoparticles further enhanced the hydrophilicity of the nanofibrous membranes. FeOOH@CS/PVA-4−12 demonstrated exceptional superhydrophilicity and underwater oleophobicity, with a water contact angle of approximately 9.5 ± 3.5° in air and an oil contact angle over 140° underwater toward oil pollutants with various viscosities (*n*-heptane, *n*-octane, and vegetable oil), leading to a remarkable separation efficiency of 98.5% and water permeation flux of 2350 $L{\cdot}m^{-2}{\cdot}h^{-1}$ during the separation of immiscible *n*-heptane/water mixtures. Furthermore, FeOOH@CS/PVA-4−12 exhibited good chemical stability and reusability, with the efficiency for *n*-heptane/water separation remaining above 97.3% after ten separation cycles and the water permeation flux remaining nearly unchanged. By further optimizing the membrane pore size from 0.48 ± 0.09 to 0.12 ± 0.03 μm, FeOOH@CS/PVA-24−24 can effectively separate *n*-heptane/water emulsions, achieving a separation efficiency of up to 99.9% and a TOC value of 8 $mg{\cdot}L^{-1}$ in the filtrate. The membrane exhibits remarkable antifouling performance, which was contributed by the superwetting surface and the photocatalytic ability of β-FeOOH nanoparticles to impart the excellent photocatalytic self-cleaning property as demonstrated by the fact that after five photocatalytic self-cleaning cycles, the water permeation flux was almost unchanged, decreasing only slightly from 546 to 522 $L{\cdot}m^{-2}{\cdot}h^{-1}{\cdot}bar^{-1}$. This indicates significant potential for practical applications.

ASSOCIATED CONTENT

Supporting Information

The Supporting Information is available free of charge at https://pubs.acs.org/doi/10.1021/acs.langmuir.4c03882.

Experimental materials, reagents, and characterization; stability of the prepared *n*-heptane−water emulsion at room temperature; swelling behavior of CS/PVA-24, CS/PVA-4, and CS/PVA-0 in water; schematic illustration of the cross-linking interaction of CS/PVA membranes; pore size distribution statistics of the membranes obtained under different conditions; stability tests of the membranes and the effects of extreme environments on the performance of the membrane materials; total organic carbon content in the filtrates after the separation of different oil-in-water emulsions; schematic diagram of the photocatalytic degradation mechanism of oil pollutants; comparison of the separation performance of the FeOOH@CS/PVA membrane with that of membranes reported in the literature (PDF)

AUTHOR INFORMATION

Corresponding Author

Zhaoxuan Feng − *State Key Laboratory of Heavy Oil Processing, College of Chemistry and Chemical Engineering, China University of Petroleum (East China), Qingdao 266580, China;* orcid.org/0000-0002-8090-088X; Email: zhaoxuan@upc.edu.cn

Authors

Hanbing Zhu − *State Key Laboratory of Heavy Oil Processing, College of Chemistry and Chemical Engineering, China University of Petroleum (East China), Qingdao 266580, China*

Yi Song − *State Key Laboratory of Heavy Oil Processing, College of Chemistry and Chemical Engineering, China University of Petroleum (East China), Qingdao 266580, China*

Haowen Qing − *State Key Laboratory of Heavy Oil Processing, College of Chemistry and Chemical Engineering, China University of Petroleum (East China), Qingdao 266580, China*

Mengying Liu − *State Key Laboratory of Heavy Oil Processing, College of Chemistry and Chemical Engineering, China University of Petroleum (East China), Qingdao 266580, China*

Yanning Zhao − *State Key Laboratory of Heavy Oil Processing, College of Chemistry and Chemical Engineering, China University of Petroleum (East China), Qingdao 266580, China*

Mingbo Wu − *State Key Laboratory of Heavy Oil Processing, College of New Energy, China University of Petroleum (East China), Qingdao 266580, China;* orcid.org/0000-0003-0048-778X

Complete contact information is available at: https://pubs.acs.org/10.1021/acs.langmuir.4c03882

Notes

The authors declare no competing financial interest.

https://doi.org/10.1021/acs.langmuir.4c03882
Langmuir 2025, 41, 633−645

■ ACKNOWLEDGMENTS

This work was supported by the financial support from the National Natural Science Foundation of China (No. 52002401) and Zhongke Derun Co., Ltd.

■ REFERENCES

(1) Cheng, Q.-Y.; Zhao, X.; Weng, Y.; Li, Y.; Zeng, J. Fully Sustainable, Nanoparticle-Free, Fluorine-Free, and Robust Superhydrophobic Cotton Fabric Fabricated via an Eco-Friendly Method for Efficient Oil/Water Separation. *ACS Sustainable Chem. Eng.* **2019**, *7* (18), 15696−15705.

(2) Wang, B.; Liang, W.; Guo, Z.; Liu, W. Biomimetic superlyophobic and super-lyophilic materials applied for oil/water separation: a new strategy beyond nature. *Chem. Soc. Rev.* **2015**, *44* (1), 336−361.

(3) Feng, Z.; Xu, Y.; Ding, W.; Li, Q.; Zhao, X.; Wei, X.; Hakkarainen, M.; Wu, M. Nano graphene oxide creates a fully biobased 3D-printed membrane with high-flux and anti-fouling oil/water separation performance. *Chem. Eng. J.* **2024**, *485*, No. 149603.

(4) Zarghami, S.; Mohammadi, T.; Sadrzadeh, M.; Van der Bruggen, B. Superhydrophilic and underwater superoleophobic membranes - review of synthesis methods. *Prog. Polym. Sci.* **2019**, *98*, No. 101166.

(5) Liu, Y.; Bai, T.; Zhao, S.; Zhang, Z.; Feng, M.; Zhang, J.; Li, D.; Feng, L. Sugarcane-based superhydrophilic and underwater superoleophobic membrane for efficient oil-in-water emulsions separation. *J. Hazard. Mater.* **2024**, *461*, No. 132551.

(6) Chen, W.; Zhang, P.; Yu, S.; Zang, R.; Xu, L.; Wang, S.; Wang, B.; Meng, J. Nacre-inspired underwater superoleophobic films with high transparency and mechanica robustness. *Nat. Protoc.* **2022**, *17* (11), 2647−2667.

(7) Raj, A.; Rego, R. M.; Ajeya, K. V.; Jung, H.-Y.; Altalhi, T.; Neelgund, G. M.; Kigga, M.; Kurkuri, M. D. Underwater oleophobic-super hydrophilic strontium-MOF for efficient oil/water separation. *Chem. Eng. J.* **2023**, *453*, No. 139757.

(8) Usman, J.; Abba, S. I.; Baig, N.; Abu-Zahra, N.; Hasan, S. W.; Aljundi, I. H. Design and Machine Learning Prediction of In Situ Grown PDA-Stabilized MOF (UiO-66-NH_2) Membrane for Low-Pressure Separation of Emulsified Oily Wastewater. *ACS Appl. Mater. Interfaces* **2024**, *16* (13), 16271−16289.

(9) Chen, L.; Dong, H.; Pan, W.; Dai, J.; Dai, X.; Pan, J. Poly (vinyl alcohol-co-ethylene) (EVOH) modified polymer inclusion membrane in heavy rare earths separation with advanced hydrophilicity and separation property. *Chem. Eng. J.* **2021**, *426*, No. 131305.

(10) Li, J.; Du, G.; Deng, C.; Zhang, H.; Dai, L. A Rapid and Facile Preparation of PVDF-PG/KH550 Bioinspired Membrane for Efficient Separation of Oil-in-Water Emulsions. *Ind. Eng. Chem. Res.* **2024**, *63* (25), 11099−11109.

(11) Zhang, T.; Xiao, C.; Zhao, J.; Liu, X.; Ji, D.; Zhang, H. One-step facile fabrication of PVDF/graphene composite nanofibrous membrane with enhanced oil affinity for highly efficient gravity-driven emulsified oil/water separation and selective oil absorption. *Sep. Purif. Technol.* **2021**, *254*, No. 117576.

(12) Yang, J.; Li, X.; Wang, S.; Zhao, Y.; Jiang, B.; Wang, H. Hierarchical Fusiform ZnO-Constructed Nanoflowers Electrodeposited on Stainless-Steel Mesh with Switchable Wettability for On-Demand Separation of Oil-Water Emulsion and Photocatalytic Degradation for Water-Soluble Pollutants. *ACS Sustainable Chem. Eng.* **2024**, *12* (23), 8806−8819.

(13) Zhang, X.; Wang, C.; Liu, X.; Wang, J.; Zhang, C.; Wen, Y. A durable and high-flux composite coating nylon membrane for oil-water separation. *J. Cleaner Prod.* **2018**, *193*, 702−708.

(14) Feng, X.; Yu, Z.; Long, R.; Sun, Y.; Wang, M.; Li, X.; Zeng, G. Polydopamine intimate contacted two-dimensional/two-dimensional ultrathin nylon basement membrane supported RGO/PDA/MXene composite material for oil-water separation and dye removal. *Sep. Purif. Technol.* **2020**, *247*, No. 116945.

(15) Ding, Z.; Tian, Z.; Ji, X.; Dai, H.; Si, C. Bio-inspired catalytic one-step prepared R-siloxane cellulose composite membranes with highly efficient oil separation. *Adv. Compos. Hybrid Mater.* **2022**, *5* (3), 2138−2153.

(16) Bai, Z.; Jia, K.; Zhang, S.; Lin, G.; Huang, Y.; Liu, X. Surface Segregation-Induced Superwetting Separation Membranes with Hierarchical Surface Structures and Internalized Gel Networks. *Adv. Funct. Mater.* **2022**, *32* (45), No. 2204612.

(17) Baig, U.; Faizan, M.; Waheed, A. A review on super-wettable porous membranes and materials based on bio-polymeric chitosan for oil-water separation. *Adv. Colloid Interface Sci.* **2022**, *303*, No. 102635.

(18) Zhang, Q.; Chen, Y.; Wei, P.; Zhong, Y.; Chen, C.; Cai, J. Extremely strong and tough chitosan films mediated by unique hydrated chitosan crystal structures. *Mater. Today* **2021**, *51*, 27−38.

(19) Doan, H. N.; Vo, P. P.; Baggio, A.; Negoro, M.; Kinashi, K.; Fuse, Y.; Sakai, W.; Tsutsumi, N. Environmentally Friendly Chitosan-Modified Polycaprolactone Nanofiber/Nanonet Membrane for Controllable Oil/Water Separation. *ACS Appl. Polym. Mater.* **2021**, *3* (8), 3891−3901.

(20) Feng, S.; Zhao, J.; Zhang, P.; Gao, Y.; Yun, J. Superhydrophilic/underwater superoleophobic oil-in-water emulsion separation membrane modified by the co-deposition of polydopamine and chitosan-tripolyphosphate nanoparticles. *J. Environ. Chem. Eng.* **2022**, *10* (3), No. 107407.

(21) Oh, S.; Bang, J.; Jin, H.-J.; Kwak, H. W. Green Fabrication of Underwater Superoleophobic Biopolymeric Nanofibrous Membranes for Effective Oil-Water Separation. *Adv. Fiber Mater.* **2023**, *5* (2), 603−616.

(22) Wang, X.; Hassan, A.; Boudaoud, H.; Xue, F.; Zhou, Z.; Liu, X. A review on 3D printing of bioinspired hydrophobic materials: oil-water separation, water harvesting, and diverse applications. *Adv. Compos. Hybrid Mater.* **2023**, *6* (5), No. 170.

(23) Feng, Z.; Xu, Y.; Yue, W.; Adolfsson, K. H.; Wu, M. Recent progress in the use of graphene/polymer composites to remove oil contaminants from water. *New Carbon Mater.* **2021**, *36* (2), 235−248.

(24) Shi, S.; Si, Y.; Han, Y.; Wu, T.; Iqbal, M. I.; Fei, B.; Li, R. K. Y.; Hu, J.; Qu, J. Recent Progress in Protective Membranes Fabricated via Electrospinning: Advanced Materials, Biomimetic Structures, and Functional Applications. *Adv. Mater.* **2022**, *34* (17), No. 2107938.

(25) Yang, G.; Li, X.; He, Y.; Ma, J.; Ni, G.; Zhou, S. From nano to micro to macro: Electrospun hierarchically structured polymeric fibers for biomedical applications. *Prog. Polym. Sci.* **2018**, *81*, 80−113.

(26) Su, Y.; Fan, T.; Cui, W.; Li, Y.; Ramakrishna, S.; Long, Y. Advanced Electrospun Nanofibrous Materials for Efficient Oil/Water Separation. *Adv. Fiber Mater.* **2022**, *4* (5), 938−958.

(27) Zhu, F.; Zhan, Y.; Chen, X.; Chen, Y.; Lei, Y.; Jia, H.; Li, Y.; Duan, X. Photocatalytic PAN Nanofibrous Membrane through Anchoring a Nanoflower-Branched CoAl-LDH@PANI Heterojunction for Organic Hazards Degradation and Oil-Containing Emulsified Wastewater Separation. *Langmuir* **2024**, *40* (28), 14368−14383.

(28) Holade, Y.; Kavousi, Z. H.; Ghorbanloo, M.; Masquelez, N.; Tingry, S.; Cornu, D. Design of three-dimensional electrocatalytic all-in-one electrodes by leveraging electrospinning and calcination approaches. *Chem. Commun.* **2022**, *59* (1), 47−50.

(29) Wang, C.; Wang, X.; Yu, J.; Ding, B. Highly Transparent Carbon Nanofibrous Membranes Inspired by Dragonfly Wings. *ACS Nano* **2023**, *17* (11), 10888−10897.

(30) Das, P.; Ojah, N.; Kandimalla, R.; Mohan, K.; Gogoi, D.; Dolui, S. K.; Choudhury, A. J. Surface modification of electrospun PVA/chitosan nanofibers by dielectric barrier discharge plasma at atmospheric pressure and studies of their mechanical properties and biocompatibility. *Int. J. Biol. Macromol.* **2018**, *114*, 1026−1032.

(31) Feng, Z.; Hakkarainen, M.; Gruetzmacher, H.; Chiappone, A.; Sangermano, M. Photocrosslinked Chitosan Hydrogels Reinforced with Chitosan-Derived Nano-Graphene Oxide. *Macromol. Chem. Phys.* **2019**, *220* (13), No. 1900174.

(32) Zhu, T.; Zhao, X.; Yi, M.; Xu, S.; Wang, Y. Ternary cross-linked PVA-APTES-ZIF-90 membrane for enhanced ethanol dehydration performance. *Adv. Compos. Hybrid Mater.* **2022**, *5* (1), 91−103.

(33) Santos, C.; Silva, C. J.; Buettel, Z.; Guimaraes, R.; Pereira, S. B.; Tamagnini, P.; Zille, A. Preparation and characterization of

polysaccharides/PVA blend nanofibrous membranes by electrospinning method. *Carbohydr. Polym.* **2014**, *99*, 584−592.
(34) Liu, Z.; Wang, B.-B.; Deng, J.-W.; Li, H.-R. One-step facile fabrication of $Mg(OH)_2$/PVA/ZnO membrane with superior stability and oil-water separation. *Sep. Purif. Technol.* **2024**, *351*, No. 128105.
(35) Han, Z.; Li, B.; Mu, Z.; Niu, S.; Zhang, J.; Ren, L. Energy-Efficient Oil-Water Separation of Biomimetic Copper Membrane with Multiscale Hierarchical Dendritic Structures. *Small* **2017**, *13* (34), No. 1701121.
(36) Chen, X.; Li, Q.; Zhang, T.; Zhen, Y.; Li, T.; Zhu, Y.; Ti, B. Benzoxazine/ thermoplastic polyurethane nanofibrous membranes with superior mechanical properties for efficient oil-water separation. *J. Membr. Sci.* **2024**, *702*, No. 122788.
(37) Fan, J.-P.; Luo, J.-J.; Zhang, X.-H.; Zhen, B.; Dong, C.-Y.; Li, Y.-C.; Shen, J.; Cheng, Y.-T.; Chen, H.-P. A novel electrospun β-CD/CS/PVA nanofiber membrane for simultaneous and rapid removal of organic micropollutants and heavy metal ions from water. *Chem. Eng. J.* **2019**, *378*, No. 122232.
(38) Chen, C.; Lu, L.; Fei, L.; Xu, J.; Wang, B.; Li, B.; Shen, L.; Lin, H. Membrane-catalysis integrated system for contaminants degradation and membrane fouling mitigation: A review. *Sci. Total Environ.* **2023**, *904*, No. 166220.
(39) Long, C.; Long, X.; Cai, Y.; Wang, X.; Li, C.; Qing, Y.; Zhao, Y. Long-lived nanoparticle-embedded superhydrophobic membranes with rapid photocatalytic properties and continuous oil-water separation. *Chem. Eng. J.* **2024**, *482*, No. 148743.
(40) Wang, H.; Wang, F.; Li, Z.; Zheng, Y.; Gu, T.; Zhang, R.; Jiang, Z. In situ reaction enabled surface segregation toward dual-heterogeneous antifouling membranes for oil-water separation. *J. Hazard. Mater.* **2023**, *460*, No. 132425.
(41) Wang, J. M.; Li, X. X.; Cheng, Q. Y.; Lv, F. Z.; Chang, C. Y.; Zhang, L. N. Construction of β-FeOOH@tunicate cellulose nanocomposite hydrogels and their highly efficient photocatalytic properties. *Carbohydr. Polym.* **2020**, *229*, No. 115470.
(42) Zeng, S.; Gao, X. J.; Chen, H. Y.; Wang, Q. T.; Si, J. H.; Cui, Z. X. Phytic acid metal complex as precursor for fabrication of superhydrophilic membrane with photo-Fenton self-cleaning property for microalgae dewatering and oil/water emulsion separation. *Sep. Purif. Technol.* **2024**, *350*, No. 127802.
(43) Yang, Y. D.; Huang, Q.; Sun, Q. H.; Xue, J. H.; Xu, S. J.; Mao, L. J.; Zhou, X. M.; Yu, D.; Li, Q. P.; Qian, J. J. Fe-Induced Coordination Environment Regulation in MOF-Derived Carbon Materials for Reduction. *ACS Sustainable Chem. Eng.* **2022**, *10*, 8641−8649.
(44) Yang, Y.; Li, X.; Zheng, X.; Chen, Z.; Zhou, Q.; Chen, Y. 3D-Printed Biomimetic Super-Hydrophobic Structure for Microdroplet Manipulation and Oil/Water Separation. *Adv. Mater.* **2018**, *30* (9), No. 1704912.
(45) Liu, M.; Wang, S.; Jiang, L. Nature-inspired superwettability systems. *Nat. Rev. Mater.* **2017**, *2* (7), 8230−8293.
(46) Zhang, H.; Wang, F.; Guo, Z. The antifouling mechanism and application of bio-inspired superwetting surfaces with effective antifouling performance. *Adv. Colloid Interface Sci.* **2024**, *325*, No. 103097.
(47) Sun, Z.; Zhang, Y. X.; Guo, S. T.; Shi, J. M.; Shi, C.; Qu, K. Q.; Qi, H. J.; Huang, Z. H.; Murugadoss, V.; Huang, M. N.; Guo, Z. Confining FeNi nanoparticles in biomass-derived carbon for effectively photo-Fenton catalytic reaction for polluted water treatment. *Adv. Compos. Hybrid Mater.* **2022**, *5* (2), 1566−1581.
(48) Dudek, G.; Turczyn, R.; Konieczny, K. Robust poly(vinyl alcohol) membranes containing chitosan/chitosan derivatives microparticles for pervaporative dehydration of ethanol. *Sep. Purif. Technol.* **2020**, *234*, No. 116094.
(49) Lachowicz, D.; Kmita, A.; Wirecka, R.; Berent, K.; Szuwarzynski, M.; Zapotoczny, S.; Pajdak, A.; Cios, G.; Mazur-Panasiuk, N.; Pyrc, K.; Bernasik, A. Aerogels based on cationically modified chitosan and poly(vinyl alcohol) for efficient capturing of viruses. *Carbohydr. Polym.* **2023**, *312*, No. 120756.
(50) Juby, K. A.; Dwivedi, C.; Kumar, M.; Kota, S.; Misra, H. S.; Bajaj, P. N. Silver nanoparticle-loaded PVA/gum acacia hydrogel: Synthesis, characterization and antibacterial study. *Carbohydr. Polym.* **2012**, *89* (3), 906−913.
(51) Garnica-Palafox, I. M.; Sanchez-Arevalo, F. M. Influence of natural and synthetic crosslinking reagents on the structural and mechanical properties of chitosan-based hybrid hydrogels. *Carbohydr. Polym.* **2016**, *151*, 1073−1081.
(52) Cheng, P.-I.; Hong, P.-D.; Lee, K.-R.; Lai, J.-Y.; Tsai, Y.-L. High permselectivity of networked PVA/GA/CS-Ag^+-membrane for dehydration of Isopropanol. *J. Membr. Sci.* **2018**, *564*, 926−934.
(53) Yang, E.; Kim, M.; Liang, Y.; Byun, J.; Kim, H.; Kim, J.; Choi, H. Tailoring the pore size of intermolecular cross-linked PIMs-based thin-film composite hollow fiber membranes using different length cross-linkers for organic solvent nanofiltration. *Chem. Eng. J.* **2023**, *474*, No. 145339.
(54) Deng, S.; Jia, S.; Deng, X.; Qing, Y.; Luo, S.; Wu, Y. New insight into island-like structure driven from hydroxyl groups for high-performance superhydrophobic surfaces. *Chem. Eng. J.* **2021**, *416*, No. 129078.
(55) Li, B.; Qian, X.; Ran, L.; Han, J.; Yang, C.; Jiao, T. Applications and challenges of superwetted oil-water separation membranes in air under liquids and in specific environments. *Prog. Org. Coat.* **2024**, *195*, No. 108673.
(56) Sreedhar, N.; Kumar, M.; Al Jitan, S.; Thomas, N.; Palmisano, G.; Arafat, H. A. 3D printed photocatalytic feed spacers functionalized with β-FeOOH nanorods inducing pollutant degradation and membrane cleaning capabilities in water treatment. *Appl. Catal., B* **2022**, *300*, No. 120318.
(57) Yue, J.; Jiang, X.; Yu, A. Experimental and theoretical study on the β-FeOOH nanorods: growth and conversion. *J. Nanopart. Res.* **2011**, *13* (9), 3961−3974.
(58) Lee, J.-T.; Yan, Z.-C.; Lin, K.-H.; Hsiao, P.-H.; Liao, P.-C.; Pu, Y.-C.; Chen, C.-Y. Co-modification of WO_3 nanoplates with β-FeOOH/carbon quantum dots combined with plasma treatment enables high-efficiency photoelectrochemical characteristics. *J. Mater. Chem. A* **2024**, *12* (30), 19277−19287.
(59) Zhang, Y.; Cui, J.; Sun, H.; Xie, A.; Li, C.; Xue, C.; Pan, J. Superwetting polypropylene fiber membrane modified with Co-doped β-FeOOH nanorods for enhanced oil/water separation and self-cleaning. *Mater.Today Chem.* **2024**, *38*, No. 102050.
(60) Tian, S.; Zhang, Y.; Sha, Q.; Zhang, X.; Yang, T.; Yan, X.; Han, N. PPS/TA-PEI/β-FeOOH membranes with powerful photo-Fenton self-cleaning capability for efficient oil-water emulsion separation. *Chem. Eng. J.* **2024**, *485*, No. 150069.
(61) Battiston, L. L.; Oliveira, K. D.; Liao, L. M.; Oliveira, G. A. R.; Kolicheski, M. B.; Avila-Neto, C. N. Towards a Correlation Between Iron/Cobalt Content, Support Pore Size and Metal Particle Size in Supported Catalysts. *Chemnanomat* **2023**, *9* (10), No. 2300264.
(62) Kong, X.; Hu, Y.; Wang, X.; Pan, W. Effect of surface morphology on wettability conversion. *J. Adv. Ceram.* **2016**, *5* (4), 284−290.
(63) Ma, S.; Lin, L.; Wang, Q.; Zhang, Y.; Zhang, H.; Gao, Y.; Xu, L.; Pan, F.; Zhang, Y. Modification of Supramolecular Membranes with 3D Hydrophilic Slide-Rings for the Improvement of Antifouling Properties and Effective Separation. *ACS Appl. Mater. Interfaces* **2019**, *11* (31), 28527−28537.
(64) Li, F.; Gao, R.; Wu, T.; Li, Y. Role of layered materials in emulsified oil/water separation and anti-fouling performance of modified cellulose acetate membranes with hierarchical structure. *J. Membr. Sci.* **2017**, *543*, 163−171.
(65) Wang, Y.; Wei, J.; Wang, Y.; Nian, P.; Wang, W.; Wei, D.; Xu, N.; Zhu, T.; Wu, Z.; Wei, Y. Insights into boosting SiC membrane superhydrophobic-superoleophilic property and oil purification performance by hierarchical structure control. *J. Environ. Chem. Eng.* **2023**, *11* (3), No. 109991.
(66) Dou, Y.-L.; Yue, X.; Lv, C.; Yasin, A.; Hao, B.; Su, Y.; Ma, P. Dual-responsive polyacrylonitrile-based electrospun membrane for

https://doi.org/10.1021/acs.langmuir.4c03882
Langmuir 2025, 41, 633−645

controllable oil-water separation. *J. Hazard. Mater.* **2022**, *438*, No. 129565.
(67) Li, H.; Zhang, J.; Gan, S.; Liu, X.; Zhu, L.; Xia, F.; Luo, X.; Xue, Q. Bioinspired Dynamic Antifouling of Oil-Water Separation Membrane by Bubble-Mediated Shape Morphing. *Adv. Funct. Mater.* **2023**, *33* (26), No. 2212582.
(68) Tummons, E.; Han, Q.; Tanudjaja, H. J.; Hejase, C. A.; Chew, J. W.; Tarabara, V. V. Membrane fouling by emulsified oil: A review. *Sep. Purif. Technol.* **2020**, *248*, No. 116919.
(69) Zakuwan, S. Z.; Ahmad, I.; Tahrim, N. A.; Mohamed, F. Functional Hydrophilic Membrane for Oil-Water Separation Based on Modified Bio-Based Chitosan-Gelatin. *Polymers* **2021**, *13* (7), No. 13071176.
(70) Gao, D.; Xin, B.; Newton, M. A. A. Preparation and characterization of electrospun PVDF/PVP/SiO2 nanofiber membrane for oil-water separation. *Colloids Surf., A* **2023**, *676*, No. 132153.
(71) Karki, H. P.; Kafle, L.; Ojha, P. D.; Song, J. H.; Kim, H. J. Cellulose/polyacrylonitrile electrospun composite fiber for effective-separation of the surfactant-free oil-in-water mixture under a versatile condition. *Sep. Purif. Technol.* **2019**, *210*, 913−919.
(72) Jiang, X.; Zhou, B.; Wang, J. Super-wetting and self-cleaning polyvinyl alcohol/sodium alginate nanofiber membrane decorated with MIL-88A(Fe) for efficient oil/water emulsion separation and dye degradation. *Int. J. Biol. Macromol.* **2023**, *253*, No. 127205.
(73) Istenič, D.; Bodik, I.; Merisaar, M.; Gajewska, M.; Seres, M.; Bulc, T. G. Challenges and Perspectives of Nature-Based Wastewater Treatment and Reuse in Rural Areas of Central and Eastern Europe. *Sustainability* **2023**, *15* (10), No. 8145.
(74) Banti, D. C.; Tsangas, M.; Samaras, P.; Zorpas, A. LCA of a Membrane Bioreactor Compared to Activated Sludge System for Municipal Wastewater Treatment. *Membranes* **2020**, *10* (12), No. 10120421.
(75) Wang, D.; Huang, L.; Sun, H.; Li, S.; Wang, G.; Zhao, R.; Zhou, S.; Sun, X. Enhanced photogenic self-cleaning of superhydrophilic Al2O3@GO-TiO2 ceramic membranes for efficient separation of oil-in-water emulsions. *Chem. Eng. J.* **2024**, *486*, No. 150211.

https://doi.org/10.1021/acs.langmuir.4c03882
Langmuir 2025, 41, 633−645